Acta Pharmaceutica Sinica B 2020;10(9):1694−1708

Chinese Pharmaceutical Association
Institute of Materia Medica, Chinese Academy of Medical Sciences

Acta Pharmaceutica Sinica B

www.elsevier.com/locate/apsb
www.sciencedirect.com

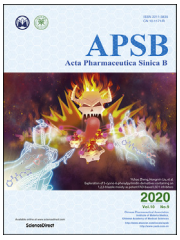

ORIGINAL ARTICLE

Identification of bioactive anti-angiogenic components targeting tumor endothelial cells in Shenmai injection using multidimensional pharmacokinetics

Chongjin Zhong[a,†], Chao Jiang[b,†], Suiying Ni[a,†], Qizhi Wang[a], Lingge Cheng[a], Huan Wang[a], Qixiang Zhang[a], Wenyue Liu[a], Jingwei Zhang[a], Jiali Liu[a], Mulan Wang[c], Min Jin[c], Peiqiang Shen[c], Xuequan Yao[b,*], Guangji Wang[a,*], Fang Zhou[a,*]

[a]*Key Laboratory of Drug Metabolism and Pharmacokinetics, State Key Laboratory of Natural Medicines, China Pharmaceutical University, Nanjing 210009, China*
[b]*Department of Digestive Tumor Surgery, Affiliated Hospital of Nanjing University of Chinese Medicine, Nanjing 210029, China*
[c]*Chiatai Qingchunbao Pharmaceutical Co., Ltd., Hangzhou 310023, China*

Received 25 September 2019; received in revised form 11 November 2019; accepted 5 December 2019

KEY WORDS

Shenmai injection;
Ginsenoside Rd;
Multidimensional pharmacokinetics;
Anti-angiogenic;
Tumor endothelial cell

Abstract Shenmai injection (SMI) is a well-defined herbal preparation that is widely and clinically used as an adjuvant therapy for cancer. Previously, we found that SMI synergistically enhanced the activity of chemotherapy on colorectal cancer by promoting the distribution of drugs in xenograft tumors. However, the underlying mechanisms and bioactive constituents remained unknown. In the present work, the regulatory effects of SMI on tumor vasculature were determined, and the potential anti-angiogenic components targeting tumor endothelial cells (TECs) were identified. Multidimensional pharmacokinetic profiles of ginsenosides in plasma, subcutaneous tumors, and TECs were investigated. The results showed that the concentrations of protopanaxadiol-type (PPD) ginsenosides (Rb1, Rb2/Rb3, Rc, and Rd) in both plasma and tumors, were higher than those of protopanaxatriol-type (Rg1 and Re) and oleanane-type (Ro) ginsenosides. Among PPD-type ginsenosides, Rd exhibited the greatest concentrations in tumors and TECs after repeated injection. *In vivo* bioactivity results showed that Rd suppressed neovascularization

*Corresponding authors. Tel.: +86 25 83271176; fax: +86 25 83271060.
E-mail addresses: 34164236@qq.com (Xuequan Yao), guangjiwang@hotmail.com (Guangji Wang), zf1113@163.com (Fang Zhou).
[†]These authors made equal contributions to this work.
Peer review under the responsibility of Chinese Pharmaceutical Association and Institute of Materia Medica, Chinese Academy of Medical Sciences.

https://doi.org/10.1016/j.apsb.2019.12.011

in tumors, normalized the structure of tumor vessels, and improved the anti-tumor effect of 5-fluorouracil (5FU) in xenograft mice. Furthermore, Rd inhibited the migration and tube formation capacity of endothelial cells *in vitro*. In conclusion, Rd may be an important active form to exert the anti-angiogenic effect on tumor after SMI treatment.

1. Introduction

Shenmai injection (SMI), extracted from red ginseng and ophiopogon roots[1], is a classical traditional Chinese medicine (TCM) injection. According to TCM theory, SMI formulae can be used to tonify "Qi", prevent exhaustion, nourish "Yin", and replenish bodily fluids. In recent years, the application of SMI has gained more popularity on account of definite curative effects and lower incidence of adverse drug reactions. Currently, SMI is clinically used for the treatment of myocardial diseases, rheumatoid diseases, and malignant tumors[2,3]. Several studies have shown that the therapeutic effects of combined chemotherapy and SMI treatments are superior to those of chemotherapy alone, in terms of efficacy and toxicity[4,5]. In our previous study, we demonstrated that SMI could increase the delivery P-gp substrates (adriamycin and paclitaxel)[6] to tumor cells, thereby enhancing their anti-tumor effects. In the present study, SMI could also promote the anti-tumor efficiency of 5-fluorouracil (5FU), which is not P-gp substrates. Therefore, synergetic anti-tumor effect of SMI combined treatments cannot be totally attributed to inhibitory effect on P-gp. Therefore, the underlying mechanisms of SMI activity remain obscure, and the key ingredient responsible for the synergetic effects observed in combined treatments is yet to be discovered.

The growth and progression of tumors require additional supplies of nutrients and oxygen that are transported by blood vessels. Therefore, the process of new blood vessel formation from a preexisting vascular endothelium, angiogenesis, is crucial[7], and has been proposed as an important cancer treatment target. Anti-angiogenic therapies, which "normalize" the abnormal blood vessels in tumors, have been shown to improve the efficacy of chemotherapy and immunotherapy, and even enhance the drug delivery into tumor[8]. Many drugs targeting tumor angiogenesis have been authorized by U.S. Food and Drug Administration (FDA) and have produced promising results in the treatment of different malignancies[9,10]. SMI could modulate the immune system[11] and improve the function of endothelial cells[12] in coronary heart disease patients. However, it is still unknown whether this injection could regulate tumor vessels.

Ginsenosides and ophiopogonins are two major components of SMI that are regarded as the principal effective constituents. Qualitative analysis demonstrates that the constituents of SMI are more similar to those of ginseng than ophiopogon[1]. Ginsenosides include protopanoxadiols (PPD), protopanaxatriols (PPT), and oleanane, all of which are structurally similar (Supporting Information Fig. S1). Different types of ginsenosides have different effects on angiogenesis. Ginsenoside Rb1, one of the most abundant constituents of ginseng, suppresses the formation of endothelial tube-like structures *in vitro*[13]. Rb2 inhibits tumor-associated angiogenesis and tumor metastasis in B16-BL6 melanoma mice[14]. Rg3 attenuates tumor angiogenesis and inhibits endogenous vascular endothelial growth factor (VEGF) secretion[15,16]. However, PPT-type ginsenosides Rg1 and Re promote the proliferation and migration of human umbilical vein endothelial cells (HUVECs) and tube formation *in vitro*[17]. Given the effectiveness of ginsenosides in the regulation of angiogenesis, SMI presumably has an effect on tumor angiogenesis and further influences drug delivery in tumors. The present study focuses on whether SMI could inhibit the angiogenesis of tumors.

Towards an important interpretation of the link between herbal medicinal product and medicinal effects, multi-dimensional pharmacokinetic (PK) measurements may open a road by dynamic tracing the exposure of certain bioactive components from plasma to tissues and the effector cells. Although the PK behavior of SMI in rats[18,19] and dogs[20] has been fully elucidated, little is known about that in tumor-bearing mice and the relationship with its synergetic anti-tumor efficacy. In this study, we aim to quantify the main components of SMI in plasma, tumor tissues, and tumor endothelial cells of LoVo colorectal cancer xenograft mice, which will help to reveal the dominant active form targeting tumor vessels.

2. Materials and methods

2.1. Chemicals and reagents

The reference standards for ginsenoside Rb1, Rb2, Rc, Rd, Rg1, Re and Rg3 were obtained from Jilin University (Changchun, China), and standard for ginsenoside Ro was purchased from Desite Co., Ltd. (Chengdu, China). SMI was provided by Chiatai Qingchunbao Pharmaceutical Co., Ltd. (Hangzhou, China). Digoxin was from the National Institute for the Control of Pharmaceutical and Biological Products (Beijing, China). Fluorouracil injection was from KingYork Pharmaceutical Co., Ltd. (Tianjin, China). Uracil-$^{13}C,^{15}N_2$ was from USBiological (Swampscott, MA, USA). Acetonitrile of high-performance liquid chromatography (HPLC) grade were purchased from Merck (Darmstadt, Germany). Methanol was of HPLC grade (Fisher, Waltham, MA, USA). Ammonium chloride and *n*-butanol were of analytical grade. Distilled water obtained using Milli Q system (Millipore, Billerica, MA, USA) was used throughout the study.

2.2. Animals

Balb/c nude mice harboring human colorectal cancer (LoVo) xenografts (6-week-old, male, 18 ± 1 g) were purchased from Shanghai SLAC Laboratory Animal Co., Ltd. (Shanghai, China). All the animals were housed in an environmentally controlled breeding room with a room temperature of 25 °C, a relative

humidity of 50%−60%, and a 12-h light/dark cycle. Food and water were provided *ad libitum*. All of the studies were conducted in accordance with Guidelines for the Care and Use of Laboratory Animals approved by Animal Ethics Committee of China Pharmaceutical University (Nanjing, China).

2.3. Studies of xenograft tumor growth and surgery for tumor tissues

For tumor growth studies, mice were weighed and the major axis (a) and minor axis (b) of xenograft tumors were measured daily during treatment. Tumor volume (TV) was calculated using Eq. (1):

$$\mathrm{TV}\ (\mathrm{mm}^3) = 1/2 \times a \times b^2 \quad (1)$$

Experiments were performed when all tumor volumes were lager than 50 mm^3. After treatment, the mice were sacrificed and tumor xenografts were removed and weighed. Tumor inhibition was calculated using Eqs. (2) and (3):

$$\begin{aligned}&\text{Inhibition of tumor growth rate}\ (\%) = \\ &\quad (1 - \text{Tumor growth rate of treatment group}/ \\ &\quad \text{Tumor growth rate of control group}) \times 100\end{aligned} \quad (2)$$

$$\begin{aligned}&\text{Tumor growth rate}\ (\%) = \\ &[\text{Tumor volume}\ (\text{day}\ t)/\text{Tumor volume}\ (\text{day}\ 0) - 1] \times 100\end{aligned} \quad (3)$$

The removed tumor was further divided into two pieces, one was rapidly frozen in drikold and stored at −80 °C for drug concentration determination and molecular biological assays and the other one was fixed in 4% PFA for immunofluorescence staining.

2.4. Two-photon microscopy

After the injection of 10 mg/kg fluorescein isothiocyanate (FITC)-labeled dextran (Sigma−Aldrich, St. Louis, MO, USA), the mice were immediately anesthetized with pentobarbital. The skin around the tumor was carefully removed and the tumor was fixed onto self-made equipment to prevent the tremble caused by the heartbeat during observation. A 20 × lens was used for observation. Z-stacks were acquired to a depth of ∼200 μm beneath the surface of the tumor. Three-dimensional reconstruction of the tumor vessels was accomplished with ZEN software (Zeiss, Oberkochen, Germany). For the quantitative analyses, at least two random optical fields per tumor were captured.

2.5. Immunofluorescence staining

The tumors were collected and fixed in 4% paraformaldehyde at 4 °C for 8 h and dehydrated by soaking the tissues blocks in 20% and 30% sucrose solution for 24 h respectively. The tissues were embedded in optimum cutting temperature compound (Leica, Weztlar, Germany). To determine the vessel braches and calculate the tumor microvascular density, the sections of 100 μm were incubated with anti-CD31 (1:100, BD Biosciences, Franklin Lakes, NJ, USA) at 4 °C overnight and then incubated with Cy5-conjugated secondary antibody (1:200, Jackson ImmunoResearch, West Grove, PA, USA) for 1 h at 37 °C. Z-stacks of tumor vessels were acquired with confocal microscope (LSM 880, Zeiss) and three-dimensional reconstruction of the tumor vessels was accomplished with ZEN software (Zeiss). For the pericyte coverage experiment, the sections of 12 μm were incubated with anti-CD31 (1:100, BD Biosciences) and anti-α-SMA (1:100, Abcam, Cambridge, UK) overnight and then incubated with Cy5 or Cy2-conjugated secondary antibody (1:200, Jackson ImmunoResearch) for 1 h at 37 °C. The pericytes around tumor vessels were observed with confocal microscope (LSM 880, Zeiss) using airscan. For the quantitative analyses, at least two random optical fields per tumor section were captured.

2.6. Pharmacokinetic studies

Pharmacokinetic studies were carried out when tumors had reached a size of at least 50 mm^3. For single administration study, 25 mice were divided into five groups (Supporting Information Table S1) and all of them were given at a single dose of 10 mL/kg SMI by intraperitoneal injection. Blood samples (∼0.1 mL) were collected in heparin-treated tube *via* the oculi chorioideae vein at the predetermined time point 0.083, 0.167, 0.33, 0.67, 1, 2, 4, 8, 12, 24, 48 and 96 h (5 mice per time point) following administration of SMI. Five mice were sacrificed at 0.33, 2, 12, 24 and 96 h by cervical dislocation and tumor tissues were collected. For multiple administration study, 25 mice were given at a dose of 10 mL/kg SMI by intraperitoneal injection once daily for 8 days. Before the last dose, mice were divided into five groups (Supporting Information Table S2). After the administration of the last dose, blood samples were collected at each time point (0.167, 0.33, 0.67, 1, 2, 4, 8, 12, 24, 48 and 96 h). Then, mice were sacrificed at 0.33, 2, 12, 24 and 96 h and tumor tissues were collected. Blood samples were centrifuged at 8000 rpm (MiniSpin, Eppendorf, Hamburg, Germany) for 5 min to obtain plasma. Tumor tissues were dispersed at 200 mg/mL in water by sonication. Both the obtained plasma and tissue samples were stored at −20 °C until analysis.

2.7. Determination of drug concentration

2.7.1. Ginsenosides

2.7.1.1. Sample preparation. Tissue suspension (100 μL) or plasma (50 μL) was transferred into a 1.5 mL centrifuge tube, and then 10 μL of digoxin (internal standard (IS), 1 μmol/L) and 1 mL of *n*-butanol were added into each tube. The mixture was vortexed for 5 min followed by centrifugation at 10,000 rpm (Sorvall biofuge stratos, Thermo scientific, Waltham, MA, USA) for 5 min. The supernatant (800 μL) was then evaporated to dryness under a gentle stream of nitrogen. The residue was reconstituted in 100 μL of methanol. After centrifugation at 18,000 rpm (Sorvall biofuge stratos, Thermo scientific) for 5 min, 70 μL of supernatant was transferred into another test tube for another centrifugation (18,000 rpm (Sorvall biofuge stratos, Thermo scientific) for 5 min), and then 5 μL of supernatant was injected onto column for HPLC−MS analysis. Supernatants of reconstituted plasma samples were diluted twice before injected into the column to ensure concentration of each ginsenoside was in a linear range.

2.7.1.2. HPLC−MS analysis. A HPLC system consisted of a LC-10AD pump, a DGU-14 AM degasser, a Shimadzu 10ATvp auto-sampler and a CTO-10Avp column oven (Shimadzu Corporation, Kyoto, Japan) was employed to achieve simultaneous detection of all analytes. Separation was performed on a Shimadzu 2010 liquid chromatograph−mass spectrometer (Shimadzu Corporation) with a LUNA C18 column (150 mm × 2 mm, 5 μm,

Phenomenex®, Los Angeles, CA, USA). The mobile phase was consisted of 0.1 mmol/L ammonium chloride solution (A) and acetonitrile (B) and the flow rate was set at 0.2 mL/min. A gradient elution program was used as follows: 0.04 → 1.5 min, B % 25 → 25; 1.5 → 12.0 min, B% 25 → 45; 12.0 → 19.0 min, B % 45 → 90; 19.0 → 22.0 min, B% 90 → 90; 22.0 → 23.0 min, B% 90 → 25; 23.0 → 29.0 min, B% 25 → 25. Quantification was performed using SIM mode with $[M+Cl]^-$ peak which was modified from our previous method[21]: *m/z* 1143.3 for Rb1; *m/z* 1113.3 for Rb2; *m/z* 1113.3 for Rc; *m/z* 981.4 for Rd; *m/z* 835.4 for Rg1; *m/z* 981.4 for Re; *m/z* 819.3 for Rg3; *m/z* 955.3 for Ro; *m/z* 815.4 for digoxin. The concentration range in plasma was 5−2000 ng/mL for Rb1 and Rb2, 5−1000 ng/mL for Rc, Rd, Rg1, Re and Ro, and 5−500 ng/mL for Rg3. The calibration curve of all ginsenosides detected in tumor showed good linearity over the concentration range of 5−500 ng/mL.

2.7.2. 5FU

2.7.2.1. Sample preparation. Tumor tissues: 200 μL of tissue suspension was transferred into a 1.5 mL centrifuge tube, and then 1 mL of methanol (containing 10 ng/mL Uracil-^{13}C,$^{15}N_2$ as IS) was added into each tube. The mixture was vortexed for 5 min followed by centrifugation at 10,000 rpm (Sorvall biofuge stratos, Thermo scientific) for 5 min, and 800 μL of supernatant was then evaporated to dryness under a gentle stream of nitrogen. The residue was reconstituted in 200 μL of methanol. After centrifugation at 18,000 rpm (Sorvall biofuge stratos, Thermo scientific) for 5 min, 150 μL of supernatant was transferred into another test tube for another centrifugation (18,000 rpm (Sorvall biofuge stratos, Thermo scientific) for 5 min), and then 5 μL of supernatant was injected onto column for HPLC−MS/MS analysis.

Plasma: 40 μL of plasma was transferred into a 1.5 mL centrifuge tube, and then 40 μL of blank plasma and 400 μL of methanol (containing 50 ng/mL Uracil-^{13}C,$^{15}N_2$ as IS) was added into each tube. The mixture was vortexed for 5 min followed by centrifugation at 18,000 rpm (Sorvall biofuge stratos, Thermo scientific) for 5 min. The supernatant (300 μL) was transferred into another test tube for another centrifugation (18,000 rpm (Sorvall biofuge stratos, Thermo scientific) for 5 min), and then 5 μL of supernatant was injected onto column for HPLC−MS/MS analysis.

2.7.2.2. HPLC−MS/MS analysis. A Shimadzu Ultra Performace LC system (Shimadzu Corporation) was interfaced to an API 4000^+ triple quadrupole mass spectrometer (Applied Biosystems, Förster City, CA, USA) outfitted with a turbo ionspray ionization source. Instrument control, data acquisition, and analysis were performed using Analyst 1.5.2 (Applied Biosystems). The sample vials were maintained at 4 °C in a thermostatic99 autosampler. The chromatographic separation was achieved on a HP Amide LC−MS/MS Column 100 mm × 3 mm, 5 μm (ChromMatrix, Richland, WA, USA) with the column temperature set at 40 °C. The mobile phase consisted of solvent A (0.1% formic acid (*v/v*), and 2.0 mmol/L ammonium acetate in water) and solvent B (acetonitrile). The mobile phases were eluted at 0.5 mL/min following the gradient as follows: 90% B maintained for 1 min, decreased to 10% at 2 min and held for 1.5 min, increased to 90% at 4.5 min followed by 2.5 min for equilibration.

The mass spectrometer was operating at the following parameters: ionspray voltage, −4.5 kV; source temperature, 550 °C; curtain gas, 30 Arb; CAD gas, 10 Pa; nebulizer gas (GS1), 65 Arb; auxiliary gas (GS2), 70 Arb. The dwell time was set at 50 ms for each ion transition. The electrospray ionization source was operated in the negative mode. MRM monitoring conditions for 5FU was as follows: Q1, 128.8 Da; Q3, 42.1 Da; DP, −25 eV; CE, −25 eV. MRM monitoring conditions for IS was as follows: Q1, 113.9 Da; Q3, 44.0 Da; DP, −45 eV; CE, −25 eV.

2.8. Tumor endothelial cells purification

After 13-day treatment of SMI, subcutaneous xenografts from Balb/c mice were removed, cut into small pieces and digested into single cell suspension by incubating in DMEM containing 2 mg/mL collagenase Type I (Sigma−Aldrich, Darmstadt, Germany) and 0.1 mg/mL DNase I (Roche, Basel, Switzerland) for 1 h. Then cells were strained with a 40 μm nylon mesh to remove cell clumps. Cells was incubated with phycoerythrin (PE) Rat Anti-Mouse CD31 (BD Biosciences) for 1 h. Anti-R-PE Magnetic Particles (BD Biosciences) was used as the secondary antibody. The endothelial cell population in the single cell suspension was enriched by magnetic isolation and washed with buffer (BD Biosciences) for 3 times. To identify the purity of endothelial cells, cells were incubated with APC Rat Anti-Mouse CD45 (BD Biosciences) and Fixable Viability Stain 440 V (BD Biosciences). Flow-cytometry was performed on a FACSAria II SORP (BD Biosciences).

2.9. Enzyme-linked immunosorbent assay (ELISA)

At 20 min after the final treatment, tumor tissues were collected and dissected in radio-immunoprecipitation assay (RIPA). The secretion of VEGF and fibroblast growth factor (FGF) in tumors was determined *via* ELISA assay according to the manufacturer's instructions (Excell, Shanghai, China). The level of VEGF and FGF were calibrated by cellular protein content, which was determined using a BCA Protein Assay Kit (Beyotime, Nanjing, China).

2.10. Cell line

HUVEC was obtained from Promocell (Heidelberg, Germany) and maintained in Dulbecco's modifed Eagle's medium (DMEM; Gibco, Carlsbad, CA, USA) supplemented with 10% fetal bovine serum (FBS, Gibco), 100 U/mL penicillin and 100 μg/mL streptomycin (Gibco). All the cells were cultured at 37 °C with 95% humidity and 5% CO_2 gas environment (normoxia). Hypoxia gas environment is maintained with 1% O_2 and 5% CO_2.

2.11. Cell viability assay

HUVECs were treated with SMI or Rd for 24 h under normoxia or hypoxia condition. The cell viability was determined using MTT assay (Beyotime). The final cell viability of the treated cells was expressed as a percentage relative to that of the DMSO-treated cells under normoxia condition.

2.12. EDU staining

After treatment with SMI or Rd for 24 h under normoxia or hypoxia condition, HUVECs were incubated in DMEM (containing EDU) for 1 h. EDU staining was performed according to the manufacturer's instructions (Beyotime). Images were captured by Lion Heart (Bio Tec, Winooski, VT, USA).

2.13. Wound healing migration assay

When HUVECs were overgrown, scratches were drawn with sterile pipette tips. Fresh DMEM was added with SMI or Rd. Images of the scratches were captured at 0 and 24 h by Lion Heart (Biotec) after incubation under normoxia or hypoxia condition. The area of the scratches was evaluated by the software and the migration length was calculated using Eq. (4):

$$\text{Migration length } (\mu\text{m}) = (\text{Scratch area}_{\ 0\,\text{h}} - \text{Scratch area}_{\ 24\ \text{h}})/\text{Scratch length} \quad (4)$$

2.14. Capillary-like tube formation assay

After incubation with SMI or Rd for 24 h, the supernatant was collected as conditioned medium (CM). HUVECs were seeded at a density of 5×10^4 cells/well into Matrigel (BD Biosciences) coated 96-well plates and treated with CM for 5.5 h under normoxia or hypoxia condition followed by 0.5 h staining of calcein (MCE, Monmouth, NJ, USA). Tubes forming intact networks were captured by Lion Heart (Biotec) and quantified by counting the number of tubes.

2.15. Data analysis

The pharmacokinetic analysis of the eight ginsenosides in plasma and tumor was performed by a non-compartmental approach using WinNonlin Professional Edition version 2.1 (Pharsight, Princeton, NJ, USA) to calculate area under the concentration−time curve ($AUC_{0-\infty}$) and half-life ($t_{1/2}$). The maximum value of concentration (C_{max}) and time to reach C_{max} (T_{max}) were obtained directly from the experimental process.

All data are presented as mean ± SEM. The unpaired *t*-test was used to assess the difference between two groups. To examine the difference among multiple groups, one-way ANOVA followed by Tukey's multiple comparison test were conducted with GraphPad Prism 7.0. A P value < 0.05 was considered statistically significant.

3. Results

3.1. SMI enhances anti-tumor effect of 5FU and normalizes tumor vessels in LoVo colon cancer xenograft mice

To confirm the synergetic anti-tumor effect of SMI on non-P-gp substrate, combined treatment of SMI and 5FU was investigated (Fig. 1A). As shown in Fig. 1B, compared to vehicle treated group, combined treatment significantly suppressed tumor growth (65.1%) compared to 5FU (49.0%) or SMI (5.1%) monotherapy, which indicated that SMI enhanced anti-tumor effect of 5FU. The influence of SMI on tumor angiogenesis was then evaluated in LoVo colon cancer xenograft mice. After treatment with SMI for 13 days at a dose of 10 mL/kg/day (Fig. 1C), the morphology of FITC-dextran labeled tumor vessels was captured using two-photon microscopy. As presented in Fig. 1D, subcutaneous tumors in vehicle-treated mice exhibited many small, tortuous, and disordered vessel branches, compared to pruned and unbent branches in SMI-treated mice. Quantitatively, the results showed that SMI decreased microvessels by 47% and branch points by 48%. CD31 staining of 100 μm thickness slides further confirmed that SMI reduced the number of microvessels and vessel branches in xenograft tumor tissues (Fig. 1E). Moreover, double-staining of CD31 and pericyte marker α-SMA showed that SMI increased pericyte coverage around tumor vessels by 1.6-fold (Fig. 1F), which is indicative of more mature vessels. These results were confirmed by thick slide (thickness = 100 μm) immunofluorescence staining (Fig. 1F).

3.2. Pharmacokinetic behavior of ginsenoside monomers in plasma after single or multiple administration of SMI

Intraperitoneal SMI injections were applied when all subcutaneous tumors had reached a size of at least 50 mm^3. Previous study demonstrated that the detectable components in plasma after treatment of SMI were very similar to that after treatment of ginseng extraction while ophiopogon extract could not be detected[1]. Therefore, our study focused on the ginsenosides in SMI. After a single dose of SMI, the concentration levels of Rb1, Rb2/Rb3, Rc, Rd, Rg3, Re, Rg1, and Ro were detected in plasma at 5, 10, 20 and 40 min, 1, 2, 4, 8, 12, 24 48 and 96 h. The temporal variations in the concentrations of these ginsenosides are illustrated in Fig. 2A. C_{max} values of Rb1, Rb2/Rb3, Rc, Rd, Rg3, Re, Rg1, and Ro were found to be 20.6, 10.1, 7.8, 3.2, 0.1, 1.6, 2.0, and 3.9 μg/mL, respectively. Maximum concentrations of Rb2/Rb3, Rc, and Rd were attained at 4 h, whereas those of Rb1, Rg3, and Ro were achieved at 1 h. Re and Rg1 maximum concentrations were observed only 10 min after SMI injection. Fig. 2B depicts the concentration−time profiles measured after eight days of SMI treatment. Maximum concentrations of Rb1, Rb2/Rb3, Rc, and Rd were achieved at 2 h, and were found to be 49.4, 21.5, 16.9, and 10.4 μg/mL, respectively. Meanwhile, the C_{max} values of Rg3 and Ro were both recorded at 20 min, and were equivalent to 0.3 and 3.7 μg/mL, respectively; whereas, those of Re and Rg1 were 1.3 and 2.1 μg/mL, respectively, recorded at 10 min.

Rb1, Rb2/Rb3, Rc and Rd were detected at all times; however, Re, Rg1, Rg3, and Ro could hardly be identified at 8 h. The $AUC_{0-\infty}$ of these ginsenosides were calculated after single or multiple SMI administration, as illustrated in Fig. 2C. The results showed that $AUC_{0-\infty}$ values of Rb1, Rb2/Rb3, Rc, and Rd were more than 20 times greater than those of Re, Rg1, Rg3, and Ro, which indicated much higher plasma exposure. Fig. 2C also shows that the AUC ratio (multiple dose/single dose) of Rd (5.28) was much greater than those of other ginsenosides (<1.87), which implied that, among these compounds, Rd accumulated the most in plasma upon multiple administration of SMI.

3.3. Pharmacokinetic behavior of ginsenoside monomers in tumors after single/multiple administration of SMI

Ginsenosides in tumors were detected at 20 min, 2, 12, 24, and 96 h after single or multiple administration of SMI. However, Re and Rg1 could only be detected at 20 min (Supporting Information Fig. S2), whereas Rg3 could not be identified at any time. The concentration−time profiles of the ginsenosides (Rb1, Rb2/Rb3, Rc, Rd, and Ro) in tumors after single or multiple SMI administration are illustrated in Fig. 3A and B.

The results showed that Ro concentrations in tumors were relatively low, and the compound could not be detected 24 h after single or multiple SMI administrations. Meanwhile, Rb1 was the most abundant ginsenoside, and Rb2/Rb3, Rc, and Rd exhibited

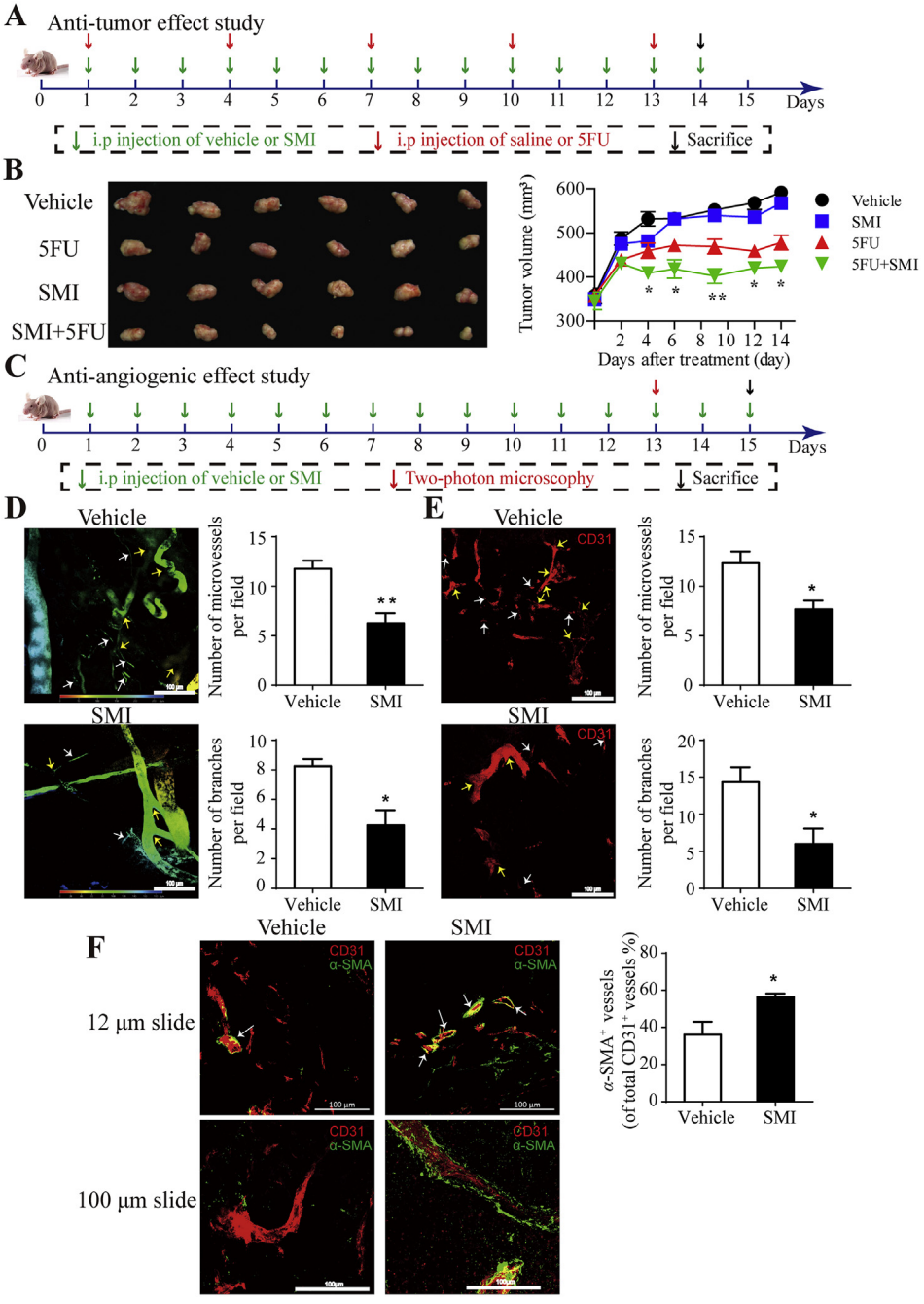

Figure 1 Effect of SMI on tumor vessels in LoVo colon cancer xenograft mice. (A) Schematic plans of animal experiments for synergic anti-tumor effect study. Mice were intraperitoneally injected with SMI (10 mL/kg/day) and 5FU (15 mg/kg/3 days) for 14 days. (B) Images and volumes of tumors dissected from mice with 14-day treatment ($n = 6$). (C) Schematic plans of animal experiments for anti-angiogenic effect study. Mice were intraperitoneally injected with SMI for 15 days. (D) Morphologies of tumor vessels captured using multi-photon laser scanning microscopy (Zeiss) after 13 days of SMI treatment. Disordered vessels and branch points are indicated by white and yellow arrows, respectively. The color represents the depth of the vessel (depth = 180−250 μm). Statistical quantification of microvessels (<10 μm in vessel diameter) and branches were in the right side of the graph ($n = 3$−4). (E) Maximum intensity projection of the Z-positions with CD31 staining of tumor vascular endothelial cells. Disordered vessels and branch points are indicated by white and yellow arrows, respectively. Statistical quantification of $CD31^+$ microvessels (<10 μm in vessel diameter) and vessel branches were shown in the right side of the graph ($n = 3$; thickness = 100 μm). (F) Double staining of CD31 (red) and α-SMA (green) of tumor slides (thickness: upper, 12 μm; lower, 100 μm). Vessels with pericyte coverage are indicated by white arrows. Statistical quantification of pericyte coverage based on calculations of the α-SMA^+ fractions was shown in the right side of the graph ($n = 3$; thickness = 12 μm). $^*P < 0.05$, $^{**}P < 0.01$ *vs.* 5FU group for B. Data were expressed as mean ± SEM. $^*P < 0.05$, $^{**}P < 0.01$ *vs.* vehicle group for D, E and F. Scale bar = 100 μm. SMI: Shenmai injection.

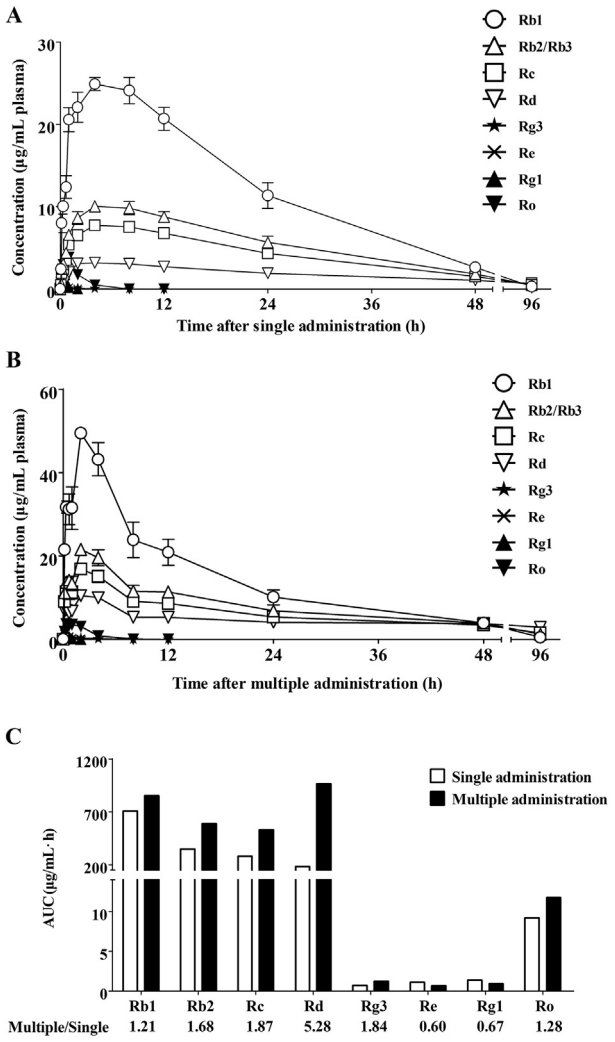

Figure 2 Concentration−time profiles of ginsenosides in plasma after single or multiple administration of SMI to Balb/c nude mice harboring LoVo xenografts. (A) and (B) Mice were intraperitoneally injected with SMI (10 mL/kg/day) once a day for one day (A) or for eight days (B). Ginsenosides in plasma were detected at 5, 10, 20 40 min, 1, 2, 4, 8, 12, 24, 48 and 96 h after the last SMI administration (n = 5 mice at each time point). (C) $AUC_{0-\infty}$ of ginsenosides in plasma after single or multiple SMI injection. The ratio between multiple and single administration was calculated to evaluate the accumulation of different ginsenosides in plasma after multiple SMI administration. Data were expressed as mean ± SEM. AUC: area under curve.

similar concentration levels, within 24 h of single dose SMI injection. Interestingly, multiple administration of SMI led to higher Rb1, Rb2/Rb3, Rc, and Rd concentrations compared to the corresponding values after single dose dispensation at all investigated time intervals. Surprisingly, multiple SMI administration resulted in much higher Rd concentrations than those of other ginsenosides.

Calculated $AUC_{0-\infty}$ values of ginsenosides in tumors, after single or multiple injections, are listed in Fig. 3C. $AUC_{0-\infty}$ of Rd was 8.0, 7.3, 3.6 and 266.6 times higher than those of Rb1, Rb2/Rb3, Rc, and Ro, respectively. The ratio of Rd between multiple to single administration was 10.53, which was also much higher than Rb1 (1.64), Rb2/Rb3 (3.33), Rc (5.67) and Ro (0.92).

3.4. *Distribution of ginsenosides in different cell populations of tumor tissues after multiple administration of SMI*

To further explore the distribution of ginsenosides in tumors, the endothelial cells in tumors were separated *via* magnetic bead sorting. Twenty mins after the last injection of 15-day SMI treatment, the tumors were dissected for the enrichment of $CD31^+$ cells and the purity was analyzed using flow-cytometry. The obtained results showed that 81.1% of the sorted live cells were endothelial cells ($CD31^+CD45^-$) (Fig. 4A). As discussed in section 3.3., seven ginsenosides were detected in the tumors, with Rd concentration being the highest. However, as shown in Fig. 4B, only four ginsenosides (Rb1, Rb2/Rb3, Rc and Rd) could be identified in TECs and non-endothelial cells. The concentration of ginsenosides in TECs were found to be higher than the corresponding values in non-endothelial cells, with Rd showing the most abundant distribution in TECs.

3.5. *Changes in constituent ratios of ginsenosides*

Temporal variations in constituent concentration ratios after single or multiple SMI injections in plasma and in tumors are presented in Fig. 5A. The ratios were calculated based on the data of Figs. 2−4. The formula is as Eq. (5):

$$\text{Ratio of ginsenoside } X = \text{Oncentration of } X / \text{Concentration of } (\text{Rb1} + \text{Rb2} + \text{Rc} + \text{Rd} + \text{Rg3} + \text{Re} + \text{Rg1} + \text{Ro}) \quad (5)$$

Higher ratios of Rd were observed after multiple SMI injections than after single injection. The Rd concentration ratio was found to be the greatest among the investigated ginsenosides in tumor tissues within 96 h after 8-day SMI injection.

The concentration ratios determined 20 min after 15-day SMI treatment for each ginsenoside in plasma, tumor tissues, and TECs are presented in Fig. 5B. The results showed that the combined ratios of PPD-type ginsenosides increased gradually in the order of SMI (59.0%), plasma (87.3%), tumor tissues (93.7%), and TECs (100%). Meanwhile, the ratios of PPT and oleanane ginsenosides decreased gradually in the same order. Among PPD-type ginsenosides, Rd ratios increased from 5.5% in SMI to 16.0% in plasma, 34.3% in tumors, and 40.3% in TECs, which rendered it the most abundant ginsenoside in TECs. In contrast, the ratios of Rb1 increased from 26.7% in SMI to 34.5% in plasma, and then decreased to 21.9% in tumors, and 14.9% in TECs.

3.6. *Ginsenoside Rd inhibits angiogenesis in vivo*

To investigate whether Rd can exert similar effects on tumor vessels *in vivo*, mice harboring LoVo xenografts were treated with SMI, Rd, Rb1, or Rg1, followed by the estimation of the number and maturity level of microvessels. The results showed that SMI and Rd-H administration, at a dose of 5 mg/kg, significantly decreased the number of microvessels (31% and 37%, respectively) and branches (40% and 59%, respectively) (Fig. 6A−C). Further evaluation demonstrated that both SMI and Rd-H increase pericyte coverage (1.8- and 2.1-fold, respectively) around microvessels (Fig. 6D and E). In contrast, Rd-L (0.5 mg/kg), Rb1, and

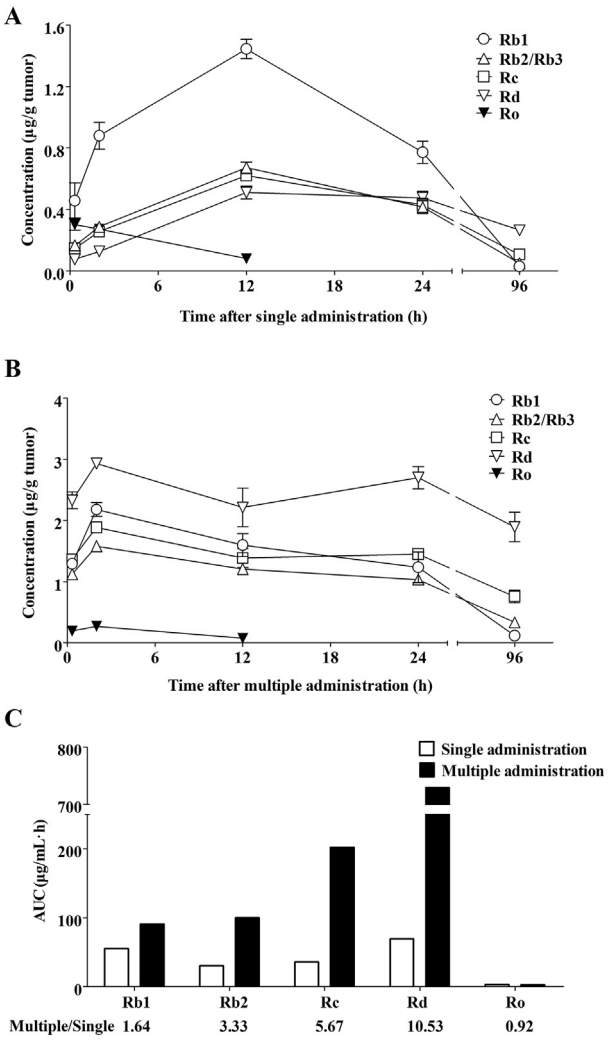

Figure 3 Concentration−time profiles of ginsenosides in tumors after single or multiple administration of SMI to Balb/c nude mice harboring LoVo xenograft. (A) and (B) Mice were intraperitoneally injected with SMI (10 mL/kg/day) once a day for one day (A) or for eight days (B). Ginsenosides in tumors were detected at 20 min, 2, 12, 24 and 96 h after the last SMI administration ($n = 5$ mice at each time point). (C) $AUC_{0-\infty}$ of ginsenosides in tumors after single or multiple SMI injection. The ratio between multiple and single administration was calculated to evaluate the accumulation of different ginsenosides in tumors after multiple SMI injections. Data were expressed as mean ± SEM.

Rg1 exhibited very modest effects on the investigated parameters compared to SMI and Rd-H (Fig. 6A−E). As shown in Fig. 6F, SMI, Rd-L, and Rd-H reduced the secretion of VEGF by 46%, 32%, and 32%, respectively, compared to modest decrease induced by Rb1 (15%) and Rg1 (1%). Moreover, SMI, Rd-H, Rb1, and Rg1 suppressed the secretion of FGF (by 68%, 68%, 99%, and 97%, respectively).

3.7. *Ginsenoside Rd inhibits angiogenesis in vitro*

HUVECs were used to confirm the anti-angiogenic effects of Rd *in vitro*. Based on the determined Rd C_{max} value of ~10 μmol/L in plasma after multiple SMI treatment, Rd concentrations in the range of 1−100 μmol/L were used to study the anti-angiogenic effects of this compound on HUVECs. As shown in Fig. 7A, Rd (1−50 μmol/L) and SMI (5 μL/mL) exhibited no effect on the cell viability of HUVECs under normoxia or hypoxia conditions. The effect of Rd, at concentrations of 2, 10, and 50 μmol/L, on cellular proliferation, migration and tube formation under hypoxia conditions similar to those observed in tumor microenvironments was also investigated. Fig. 7B and C shows that Rd has no significant effect on cellular proliferation of HUVECs. Meanwhile, Fig. 7D and E shows that HUVECs possessed enhanced migration ability (24%) under hypoxia conditions. Rd (2, 10 and 50 μmol/L) suppressed HUVECs migration concentration-dependently and almost abolished hypoxia-induced migration (88%) at 50 μmol/L concentration. Similarly, hypoxia improved the tube formation ability of HUVECs by 27%, and 2, 10, and 50 μmol/L Rd solutions inhibited this ability by 18%, 40%, and 56%, respectively (Fig. 7F and G). SMI also exhibited a repression effect on HUVECs migration and tube formation.

3.8. *Influence of ginsenoside Rd on the anti-tumor effects of chemotherapy*

Considering the profound anti-angiogenic effect of Rd on tumor vessels, further studies were performed to investigate whether this compound can improve the anti-tumor activity of chemotherapy treatments. Combinatorial administrations of SMI or Rd along with the chemotherapeutic drug for colorectal cancer, 5FU, were used to treat Balb/c mice harboring LoVo xenografts (Fig. 8A). As expected, Rd+5FU led to a greater suppression (43%) of tumor growth compared to vehicle + saline, and even compared to vehicle+5FU or SMI+5FU (17% or 26%). Meanwhile, treatments composed of SMI or Rd alone had no significant effect on tumor growth (Fig. 8B and C). The obtained results indicated that 5FU suppressed the increase of mice body weight by 65% and that SMI or Rd co-administration abolished this effect (Fig. 8D). Furthermore, all six groups of tumor-bearing mice treated with 5FU at day 20, and the concentration of 5FU in tumor tissues were measured. Although SMI or Rd alone had no significant effect on these concentrations, SMI+5FU and Rd+5FU treatments remarkably increased the level of 5FU in tumors by 57% and 54%, respectively, compared to 5FU treatment alone. Meanwhile, changes in 5FU concentrations in plasma were found to be negligible (data not shown).

4. Discussion

Many studies have reported that SMI is a safe and effective adjunct to chemotherapy in cancer interventions[3,5,22]. We have demonstrated that SMI enhanced the anti-cancer effects of P-gp substrates (adriamycin and paclitaxel)[6] and non-P-gp substrates (5FU, Fig. 1) in colon cancer xenograft mice by improving their distributions in tumors. The increased effects of SMI on intratumor concentrations of different chemotherapeutic drugs cannot be simply attributed to the inhibitory effect on P-gp. The efficiency of drug delivery in tumors is closely related to the structure and function of vessels[23,24]. For example, bevacizumab, an anti-angiogenic drug, enhances the effects of chemotherapy or radiotherapy by promoting the normalization of tumor vessels[25−27]. Since SMI has definite protective effect on cardiovascular system[2,11,12], we inferred that SMI might increase chemotherapeutic drugs through regulating the blood vessels of tumors. Therefore, we decided to investigate the effect of SMI on tumor vessels and

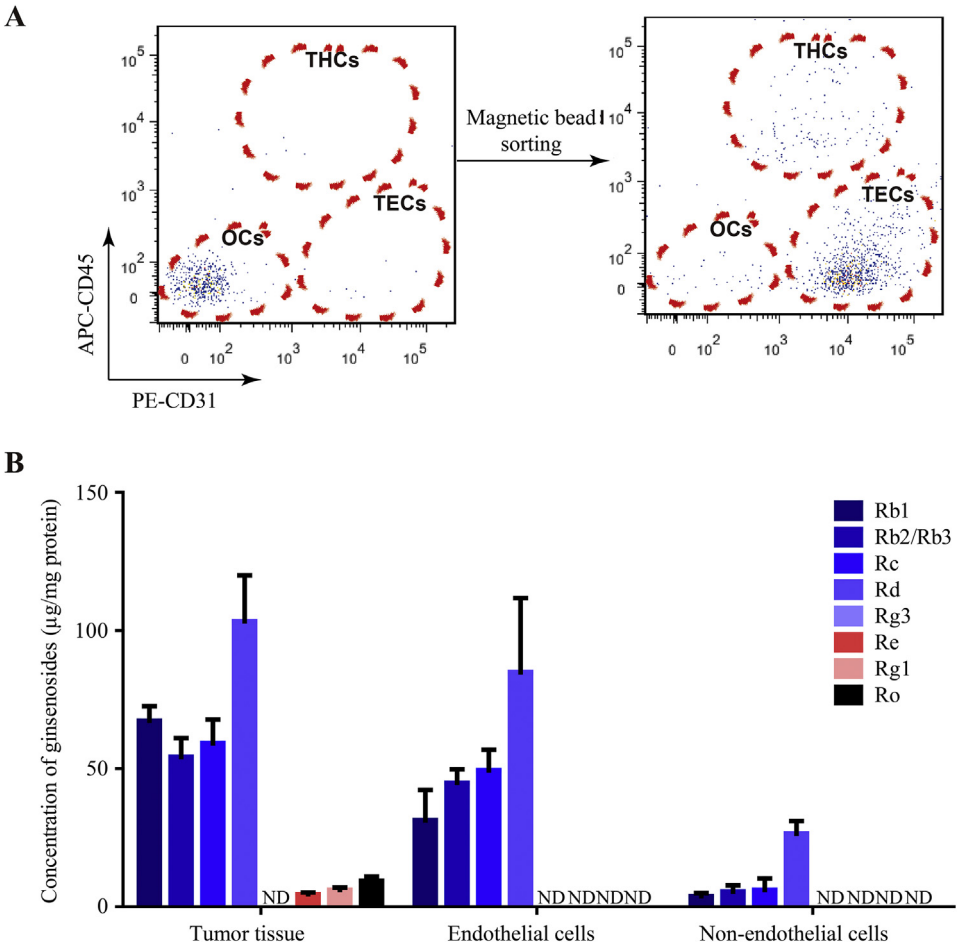

Figure 4 The concentration of ginsenosides in tumor endothelial and non-endothelial cells. (A) Identification of TECs sorted by magnetic bead using Flow-cytometry. (B) Concentration of ginsenosides in tumor endothelial or non-endothelial cells at 20 min after 15-day SMI treatment ($n = 3$). Data were expressed as mean ± SEM. TECs: tumor endothelial cells; THCs: tumor hematopoietic cells; OCs: other cells; ND, not detected.

elucidate the material basis underlying its synergetic anti-cancer activity.

In this study, we demonstrate that SMI exerts an anti-angiogenic effect and enhances the maturity of tumor microvessels. Among the numerous components of SMI, ginsenosides are regarded as the main active ingredients[1]. This study focuses on the PK behavior of ginsenoside constituents in plasma, tumor tissues, and isolated TECs in LoVo colorectal cancer xenograft mice after intraperitoneal administration of SMI. Among the 8 ginsenosides detected in plasma after SMI treatments, Rb1, Rb2/Rb3, Rc, and Rd exhibit the highest concentration levels. In light of the short half-lives of Rg3, Re, Rg1, and Ro, these components were nearly completely eliminated after 12 h of SMI administration, leading to little accumulation in plasma, even for multiple injection treatment. It is worth noting that, compared to single dose administration, PPD-type ginsenosides, namely Rb1, Rb2/Rb3, Rc, and Rd, showed obvious accumulation after multiple dose treatment, with Rd presented the highest accumulation levels and slowest elimination in plasma. The data obtained herein for xenograft mice was consistent with that reported in previous PK studies performed in rats and dogs. Within 30 min of intravenous SMI administration to rats, only 13 circulating saponins were detected and PPD-type ginsenosides (except for Rg3) exhibited higher concentrations and longer terminal half-lives in plasma[28]. In another study[20], the PK profiles of 8 ginsenosides (Rb1, Rb2, Rc, Rd, Re, Rf, Rg1 and Ro) were simultaneously determined after intravenously injecting SMI in dogs. The results demonstrated that PPD-type ginsenosides exhibited much higher concentrations and much slower elimination rates than PPT-type ginsenosides. Similar results were also observed in dogs after long-term SMI treatment[29].

The efficiency of drug transfer from plasma to the target tissues is, theoretically, one of the factors limiting the therapeutic effect[30]. Therefore, in this study, we determined the distribution of ginsenosides in tumor tissues after SMI treatment. To the best of our knowledge, no previous reports of such data exist in the literature. The obtained results showed that after multiple injections of SMI, seven out of eight ginsenosides (excluding Rg3) could be detected in tumors. However, the concentrations of Re, Rg1, and Ro were found to be relatively low, and they could hardly be detected 24 h after the last SMI administration, which indicates low exposure levels. Meanwhile, PPD-type ginsenosides (Rb1, Rb2/Rb3, Rc and Rd) were found to be accumulated in tumors, with Rd showing the highest concentrations within 96 h of multiple dose SMI treatment. Compared to other PPD type ginsenosides, Rd has a relatively lower concentration in SMI formula and plasma, but it shows the highest efficiency for the transfer from blood to tumor tissues. The AUC ratio (multiple

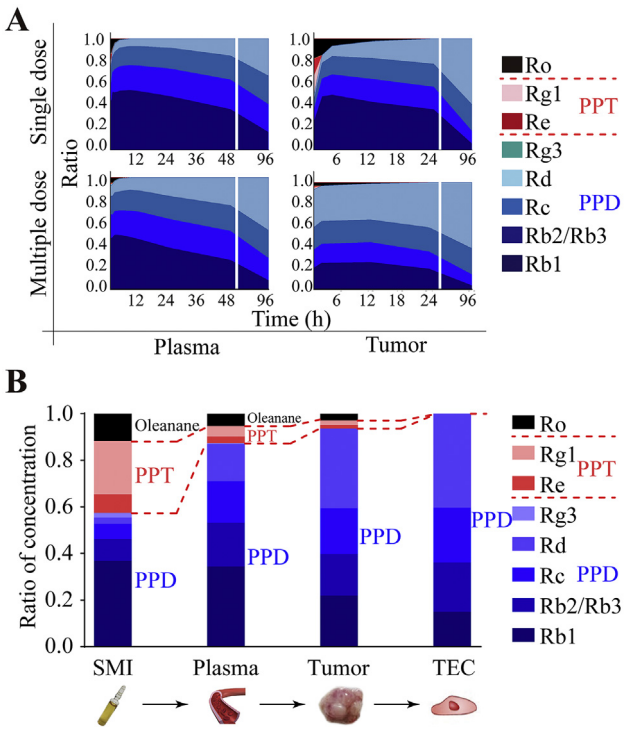

Figure 5 The accumulation of ginsenosides in plasma, tumor tissues, and endothelial cells after multiple administration of SMI to Balb/c nude mice harboring LoVo xenograft. (A) The constituent ratio−time profiles of ginsenosides in plasma and tumors after single or multiple (8-day) administration of SMI (10 mL/kg/day). (B) The constituent ratio of ginsenosides in SMI, plasma, tumor, and endothelial cell measured 20 min after 15-day SMI treatment. The ratio changes of different types of ginsenosides are separated by red dotted lines in the graph. Data were expressed as mean ± SEM. PPD: protopanaxadiol-type ginsenosides; PPT: protopanaxatriol-type ginsenosides.

dose/single dose) of Rd in tumor tissues was determined to be 10.53, which is much higher than that of other ginsenosides. The higher transfer and retention efficiencies of Rd potentially lead to higher concentrations of this compound in tumors. Further assessment showed that 20 min after the injection of the last dose in a 15-day SMI treatment, the proportions of PPD-type ginsenosides increased in the following order: SMI formula, plasma, tumor tissues, and TECs, with Rd proportions presented the greatest changes. This indicates that Rd accumulates well in tumor tissues and in TECs.

Various factors may contribute to the accumulation of Rd in tumors despite its low concentration in SMI formulae. The relatively long half-life of Rd in tumors promotes its accretion by inhibiting its elimination (Supporting Information Fig. S3). The bioconversion of Rb1 to Rd is another factor that contributes to higher concentrations of the latter in tumors. This is confirmed by the detection of higher Rd concentrations in the tumors of SMI-treated mice than in those of Rd-treated mice, despite similar Rd content in both treatments (Supporting Information Fig. S4). Moreover, both Rb1 and Rd were detected in mice treated with pure Rb1, indicating the conversion of Rb1 to Rd in plasma and tumors (Fig. S4). The biotransformation of ginsenosides was also reported for some bacterium *via* β-glucosidase[31,32]. The accumulation of Rd in tumors is also influenced by the superior uptake of Rd by HUVEC and LoVo *in vitro,* compared to Rb1 and Rb2 (Supporting Information Fig. S5). Meanwhile, many studies have shown that some components in SMI affect the PK profiles of other drugs. For example, panaxytriol in SMI affects CYP3A4-mediated 1′-hydroxylation and 4-hydroxylation of midazolam[33], and some ginsenosides influence the uptake of drugs *via* OATPs[34]. Further investigation is needed to determine whether the PK profiles of Rd or other ginsenosides could be affected by other components in SMI. In conclusion, our results show that Rd is the most accumulated ginsenoside in tumors and TECs upon multiple SMI administration, and that this compound is probably the main active component responsible for the normalization of tumor microvessels.

Angiogenesis is needed to supply nutrients and oxygen to tumor tissues, and is thus, essential for tumor growth and metastasis[7]. Pro-angiogenic signals in tumors are always over-activated due to hypoxia conditions[35]. However, the newly-formed tumor vessels are usually structurally abnormal and lack pericyte coverage, which leads to functional defectiveness, such as perturbed blood flow and leakage[36]. The activity of some anti-angiogenic drugs is based on the normalization of tumor vessels, which prevents the invasion of tumor cells and improves the anti-tumor effect of chemotherapy[37,38]. Increasing clinical data have demonstrated that many anti-angiogenic drugs combined with chemotherapy, radiotherapy or immunotherapy show better clinical efficacy than monotherapy[39,40]. Now this therapeutic strategy has been widely accepted and used by more and more doctors. Many studies have shown that anti-angiogenic drugs can normalize tumor blood vessels within a certain time window, which can improve tumor blood flow perfusion and enhance chemotherapeutic drug delivery into tumors[27,41]. This may alter the microenvironment and metabolic state of cancer cells[42], which makes them more sensitive to chemotherapy, radiotherapy or immunotherapy. In this study, we demonstrated that SMI can prune the microvessels and promote vascular maturation, which lead to improved vascular structure. Seeing as it is the most accumulated ginsenoside in tumor tissues and TECs, the effect of Rd on the regulation of tumor microvessels was investigated.

Many existing studies report that Rd suppresses the proliferation[43,44] and metastasis[45,46] of cancer cells. Recently, it was revealed that Rd also suppresses breast tumor growth and tumor angiogenesis in xenografted mice[47]. However, the effects of Rd on tumor vessels still need to be confirmed in other xenografted models, and the underlying mechanisms need to be established. These effects were evaluated for two different doses of Rd: 0.5 (low dose) and 5 mg/kg/day (high dose), which correspond to the amount of Rd in 10 mL of SMI and the accumulated amount of this compound in tumors after 15-day SMI treatment (10 mL/kg/day), respectively (Fig. S4). Since ginsenosides Rb1 and Rg1 are considered as quality control components in the process of SMI formula production, their influence on tumor vessel regulation was also investigated. The results showed that the vessels of Rd-treated mice exhibited less branches and more pericyte coverage compared to the vehicle-treated group, which indicates that Rd normalizes tumor vessels, similar to SMI. Meanwhile, Rb1 and Rg1 presented no significant regulative effect on the abnormal morphology of tumor vessels, nor on tumor growth and body weight (Supporting Information Fig. S6). The imbalance of pro- and anti-angiogenic signaling within tumors is assumed to be the switch for abnormal tumor angiogenesis. Over-activated pro-angiogenic signals can trigger tumor angiogenesis, thereby creating abnormalities in tumor

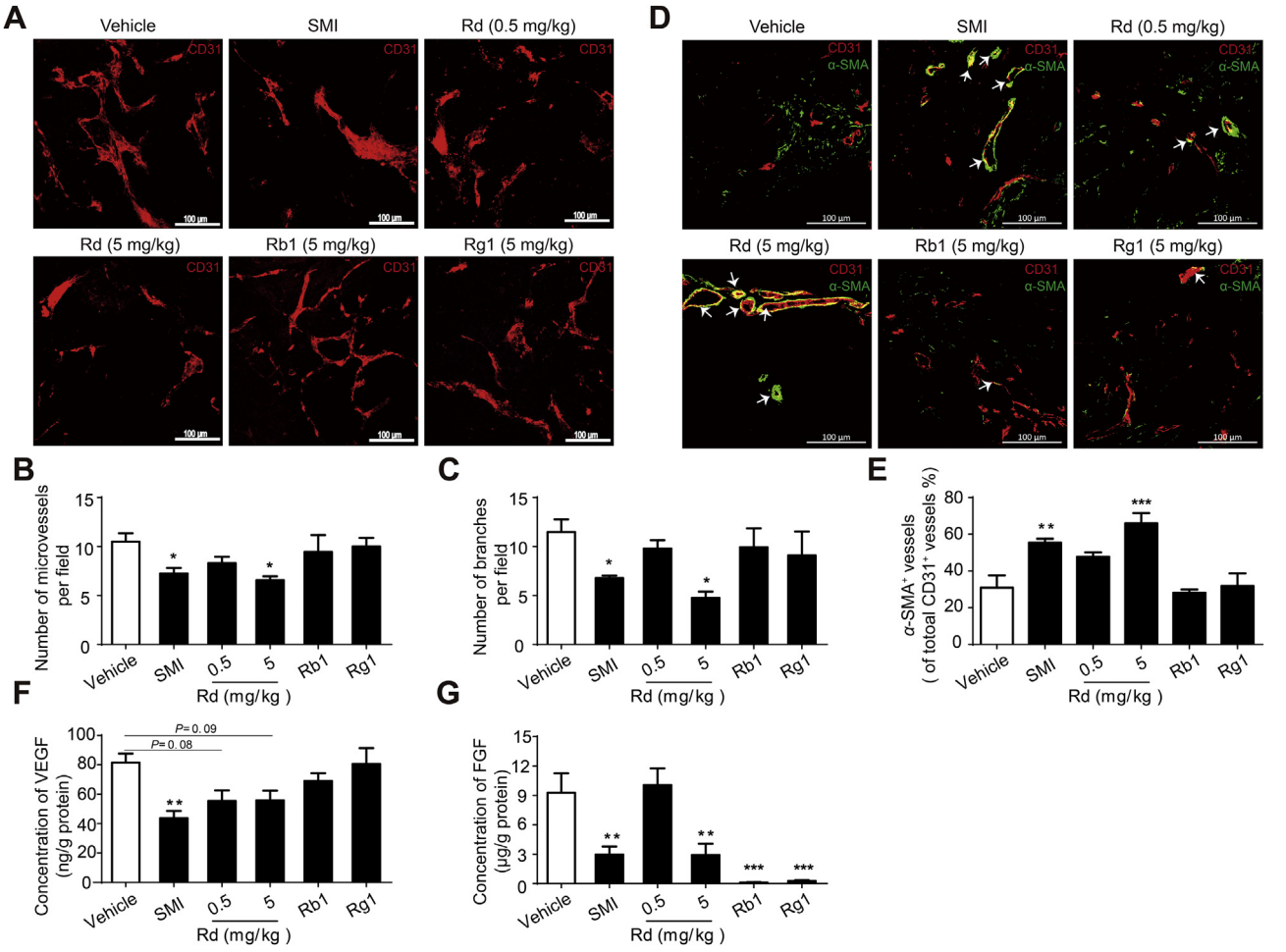

Figure 6 Effect of Rd on tumor vessels in Balb/c mice harboring LoVo xenografts. Mice were intraperitoneally injected with SMI, Rd, Rb1, Rg1, or vehicle for 15 days. Maximum intensity projection of the Z-positions with CD31 staining of tumor vascular endothelial cells (n = 3–4; thickness = 100 μm; scale bar = 100 μm). (B) and (C) Statistical quantification of $CD31^+$ microvessels (<10 μm in vessel diameter, B) and vessel branches (C) in (A). (D) Double staining of CD31 (red) and α-SMA (green) in tumors revealing pericyte coverage around tumor vessels (n = 4; thickness = 12 μm; scale bar = 100 μm). (E) Statistical quantification of pericyte coverage based on calculations of the α-SMA^+ fractions in (D). (F) and (G) The secretion level of VEGF (F) and FGF (G) in tumors (n = 6–7). Data were expressed as mean ± SEM. $^*P < 0.05$, $^{**}P < 0.01$, $^{***}P < 0.001$ *vs.* vehicle group.

microenvironments and fueling tumor progression[35]. Our data showed that 15-day Rd treatment produces effects similar to SMI treatment, with simultaneous suppression of VEGF and FGF secretion in tumors. However, Rb1 or Rg1 treatments only affect the secretion of FGF. VEGF is a major target in anti-angiogenesis treatment and its role in pathological angiogenesis is widely recognized[48]. In contrast, FGF signaling activation has been characterized as a mechanism of tumor escape in response to anti-VEGF therapy[48]. Therefore, it is not surprising that Rb1 and Rg1 significantly inhibit the secretion of FGF but cannot suppress tumor angiogenesis.

The effect of Rd on angiogenesis *in vitro* was also verified using HUVECs. The development of new blood vessels from the pre-existing vascular bed in angiogenesis is indicated by the proliferation, migration, and tube formation of endothelial cells[36]. Based on the results of PK evaluation, the C_{max} value of Rd in plasma after eight days of SMI treatment is approximately 10 μmol/L. At this concentration, Rd effectively suppresses HUVECs ability of migration and tube formation under hypoxia condition, without significant cytotoxicity.

Many studies indicate that anti-angiogenic agents can normalize tumor vasculature in a certain time window to improve the efficacy of chemotherapy, immunotherapy and even enhance the drug delivery into tumor[49,50]. The results obtained herein show that both SMI and Rd are capable of normalizing tumor vessels at a dose without directly suppressing tumor growth when used alone (Fig. S6). Furthermore, the combination of either one of them with 5FU enhances the anti-tumor effect of the latter by increasing its concentration in tumor tissues. Moreover, SMI and Rd can reverse the adverse influence of 5FU on body weight. Therefore, SMI and Rd improves the anti-tumor efficiency of 5FU and attenuates its toxicity at the same time.

Although Rd may be an important active form to exert the anti-angiogenic effect on tumor after SMI treatment, the contribution of other ginsenosides in SMI to the regulation of tumor microvessels remains unclear and cannot be completely ignored. For example, part of the detected Rd in tumors was biotransformed from Rb1 (Fig. S4). Rb1 inhibits angiogenesis by adjusting the pigmented epithelial derived factor[51]. However, the concentration of this compound in tumor tissues and endothelial cells was found to be

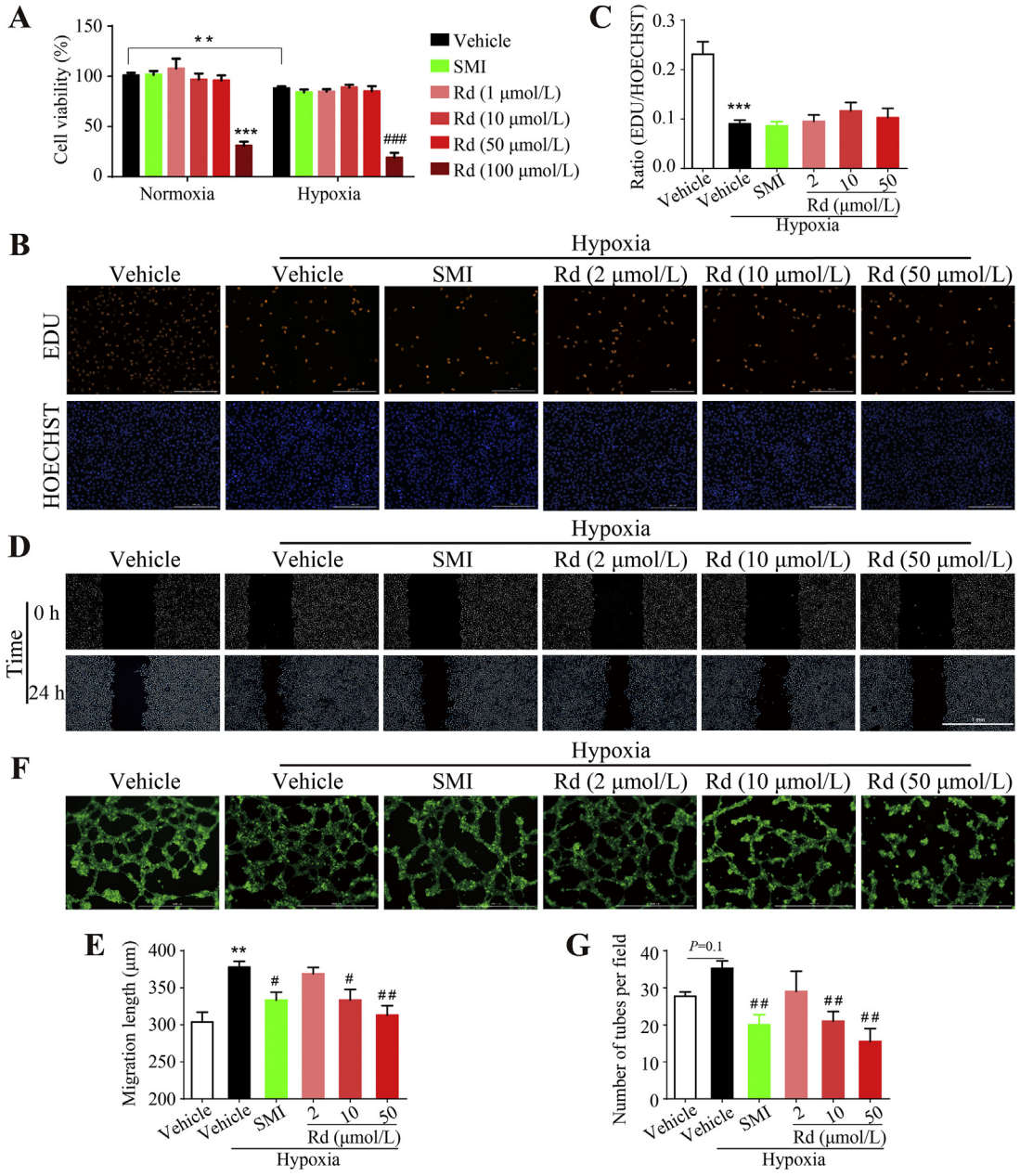

Figure 7 Effect of Rd on angiogenesis *in vitro*. (A) HUVECs were treated with SMI Rd for 24 h under normoxia or hypoxia conditions. Cell viability was tested by MTT assays ($n = 6$). (B) and (C) Rd has no significant effect on HUVEC proliferation in hypoxia condition. HUVECs were treated with SMI or Rd for 24 h followed by EDU/HOECHST staining. (B) Representative images of EDU and HOECHST. Scale bar, 200 μm. (C) Ratio of EDU/HOECHST ($n = 5$). (D) and (E) Rd represses the migration of HUVECs under hypoxia condition. HUVECs were scratched by pipette tips and treated with SMI or Rd for 24 h. (D) Representative images of wound healing at 0 and 24 h. Scale bar = 1 mm. (E) Quantification of migration length ($n = 6$). (F) and (G) Rd suppresses tube formation of HUVECs under hypoxia condition. HUVECs were pre-treated with SMI or Rd for 24 h and seeded on Matrigel for 5.5 h followed by 0.5 h of calcein staining. (F) Representative images of tubes. Scale bar = 1 mm. (G) Quantification of tubes in (D) ($n = 4$). Data were expressed as mean ± SEM. $^{**}P < 0.01$, $^{***}P < 0.001$ *vs*. normoxia + DMSO group, $^{\#}P < 0.05$, $^{\#\#}P < 0.01$, $^{\#\#\#}P < 0.001$ *vs*. hypoxia + DMSO group.

relatively low, due to conversion to Rd. Furthermore, the results obtained *in vivo* showed that the influence of Rb1 on tumor angiogenesis is far less potent than that of Rd (Fig. 6A–G). Rg1 and Re are also components of SMI that have been reported to promote angiogenesis[52,53]. However, they are quickly eliminated in plasma and tumor tissues, with little distribution in tumors. Rg3 and compound K (CK) are the major/final gut microbiome metabolites of Rb1, Rb2, Rc, and Rd[54], and they exert significant anti-angiogenic effects on various cancers[55–57]. However, neither Rg3 nor CK could be detected in plasma or tumor tissues after intraperitoneal injection of Rb1, Rc, or Rd (data not shown) in mice harboring xenograft tumors. Although the concentration levels of

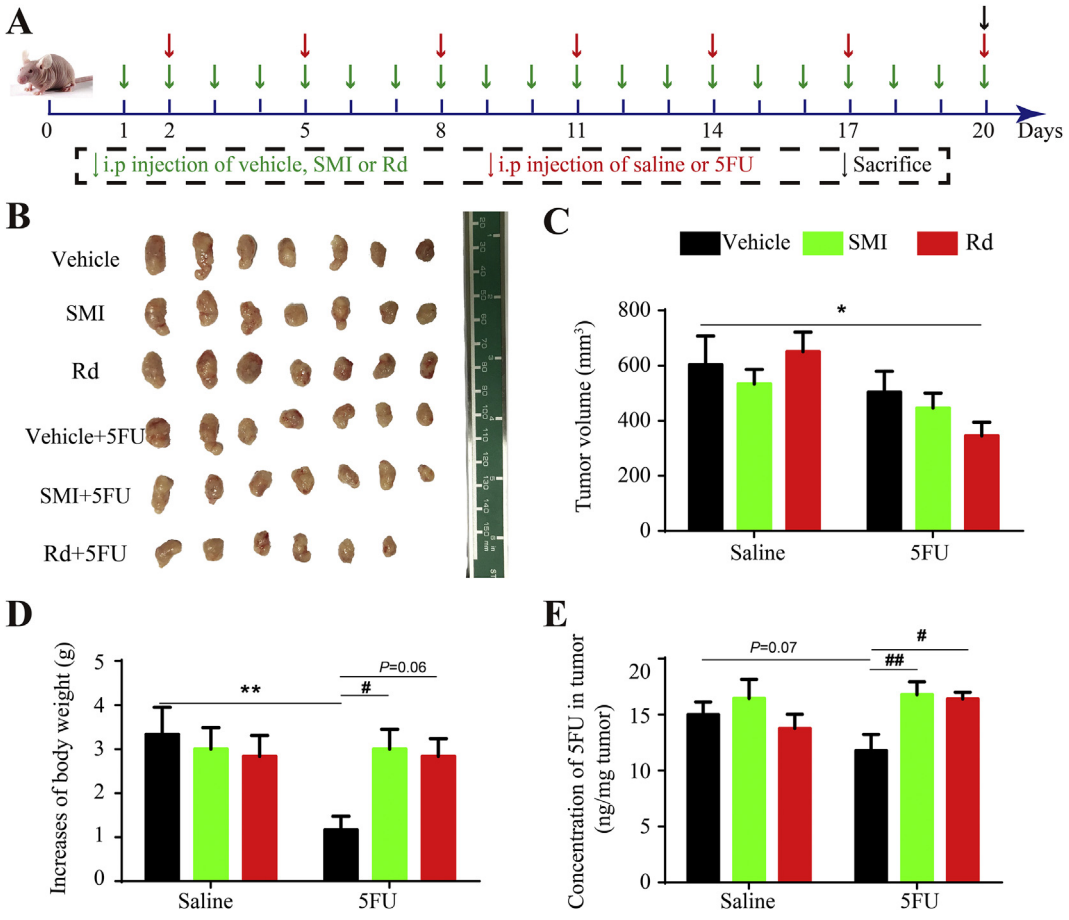

Figure 8 Influence of Rd on the anti-tumor effect of chemotherapy *in vivo*. Schematic plans of animal experiments. Mice were intraperitoneally injected with SMI (10 mL/kg/day), Rd (5 mg/kg/day) or 5FU (15 mg/kg/3 days) for 20 days. (B) and (C) SMI and Rd enhance the inhibition effect of 5FU on tumor growth. (B) Images of tumors resected from mice after 20-day treatment. (C) Tumor volumes after 20-day treatment. (D) Changes in mice body weight after 17-day treatment. (E) Concentration of 5FU in tumor tissues after 20-day treatment. Data were expressed as mean ± SEM. $^{*}P < 0.05$, $^{**}P < 0.01$ *vs*. vehicle + saline group, $^{\#}P < 0.05$, $^{\#\#}P < 0.01$ *vs*. vehicle+5FU group, $n = 6-7$.

these ginsenosides in plasma and tumors were found to be low or even below the detection limit, their contribution to the angiogenic regulatory effects of SMI still needs further investigation.

5. Conclusions

Potential active ingredients of SMI targeting tumor angiogenesis were identified using multidimensional PK experiments. The obtained results showed that Rd was the main component accumulated in tumors and TECs, and its regulatory effect on tumor angiogenesis was confirmed *in vitro* and *in vivo*. Overall, the results suggested that Rd may be an important active form to exert the anti-angiogenic effect on tumor after SMI treatment. Furthermore, this study proposed a new method for the discovery of active substances in multi-component traditional Chinese medicines using multidimensional pharmacokinetics.

Acknowledgments

This work was supported by the China National Nature Science Foundation (81573496, 81773989, 81530098 and 81573494); National Research Council of Science and Technology Major Project of China (2017ZX09201004-019 and 2019ZX09721001-006-005); International Science and Technology Center Program of China (2017YFE0109600); Foundation for Innovative Research Groups of the National Natural Science Foundation of China (No. 81421005); Jiangsu Province Nature Science Foundation (No. BK20160076, China); Jiangsu Province "333" project, China; Six talent peaks project in Jiangsu Province (YY-060), China; National Basic Research Program of China (973 Program, No. 2017YFA0205400); "Double First-Class" University project (CPU2018GF01, China).

Author contributions

Fang Zhou, Guangji Wang and Xuequan Yao designed the research. Chongjin Zhong, Chao Jiang and Suiying Ni carried out the experiments and performed data analysis. Huan Wang, Qixiang Zhang, Wenyue Liu, Qizhi Wang, Lingge Cheng, Jingwei Zhang and Jiali Liu participated part of the experiments. Mulan Wang, Min Jin and Peiqiang Shen provided experimental drugs and quality control. Fang Zhou, Chongjin Zhong and Chao Jiang wrote the manuscript. Fang Zhou, Guangji Wang and Xuequan Yao revised the manuscript. All of the authors have read and approved the final manuscript.

Conflicts of interest

The authors have no conflicts of interest to declare.

Appendix A. Supporting information

Supporting data to this article can be found online at https://doi.org/10.1016/j.apsb.2019.12.011.

References

1. Zhang HJ, Wu YJ, Cheng YJ. Analysis of 'SHENMAI' injection by HPLC/MS/MS. *J Pharm Biomed Anal* 2003;**31**:175−83.
2. Xian S, Yang Z, Lee J, Jiang Z, Ye X, Luo L, et al. A randomized, double-blind, multicenter, placebo-controlled clinical study on the efficacy and safety of Shenmai injection in patients with chronic heart failure. *J Ethnopharmacol* 2016;**186**:136−42.
3. Zhang D, Zheng J, Ni M, Wu J, Wang K, Duan X, et al. Comparative efficacy and safety of Chinese herbal injections combined with the FOLFOX regimen for treating gastric cancer in China: a network meta-analysis. *Oncotarget* 2017;**8**:68873−89.
4. Zhu WR, Zheng L, Guo YB, Yuan JM, Shen XH. Clinical research of intraperitoneal chemotherapy plus Shenmai injection in treating advanced colorectal cancer. *Zhong Xi Yi Jie He Xue Bao* 2005;**3**:266−9.
5. Wang L, Huang XE, Cao J. Clinical study on safety of cantharidin sodium and shenmai injection combined with chemotherapy in treating patients with breast cancer postoperatively. *Asian Pac J Cancer Prev APJCP* 2014;**15**:5597−600.
6. Liu WY, Zhang JW, Yao XQ, Jiang C, He JC, Ni P, et al. Shenmai injection enhances the cytotoxicity of chemotherapeutic drugs against colorectal cancers *via* improving their subcellular distribution. *Acta Pharmacol Sin* 2017;**38**:264−76.
7. Weis SM, Cheresh DA. Tumor angiogenesis: molecular pathways and therapeutic targets. *Nat Med* 2011;**17**:1359−70.
8. Petrillo S, Tolosano E, Munaron L, Genova T. Targeting metabolism to counteract tumor angiogenesis: a review of patent literature. *Recent Pat Anti-Cancer Drug Discov* 2018;**13**:422−7.
9. Simon T, Gagliano T, Giamas G. Direct effects of anti-angiogenic therapies on tumor cells: VEGF signaling. *Trends Mol Med* 2017;**23**:282−92.
10. Chung AS, Lee J, Ferrara N. Targeting the tumour vasculature: insights from physiological angiogenesis. *Nat Rev Cancer* 2010;**10**:505−14.
11. Fang T, Li J, Wu X. Shenmai injection improves the postoperative immune function of papillary thyroid carcinoma patients by inhibiting differentiation into Treg cells *via* miR-103/GPER1 axis. *Drug Dev Res* 2018;**79**:324−31.
12. Zhang YC, Lu BJ, Zhao MH, Rong YZ, Chen RM. Effect of Shengmai injection on vascular endothelial and heart functions in patients with coronary heart disease complicated with diabetes mellitus. *Chin J Integr Med* 2008;**14**:281−5.
13. Leung KW, Cheung LW, Pon YL, Wong RN, Mak NK, Fan TP, et al. Ginsenoside Rb1 inhibits tube-like structure formation of endothelial cells by regulating pigment epithelium-derived factor through the oestrogen beta receptor. *Br J Pharmacol* 2007;**152**:207−15.
14. Sato K, Mochizuki M, Saiki I, Yoo YC, Samukawa K, Azuma I. Inhibition of tumor angiogenesis and metastasis by a saponin of *Panax ginseng*, ginsenoside-Rb2. *Biol Pharm Bull* 1994;**17**:635−9.
15. Sun C, Yu Y, Wang L, Wu B, Xia L, Feng F, et al. Additive anti-angiogenesis effect of ginsenoside Rg3 with low-dose metronomic temozolomide on rat glioma cells both *in vivo* and *in vitro*. *J Exp Clin Cancer Res* 2016;**35**:32.
16. Chen QJ, Zhang MZ, Wang LX. Gensenoside Rg3 inhibits hypoxia-induced VEGF expression in human cancer cells. *Cell Physiol Biochem* 2010;**26**:849−58.
17. Yu LC, Chen SC, Chang WC, Huang YC, Lin KM, Lai PH, et al. Stability of angiogenic agents, ginsenoside Rg1 and Re, isolated from Panax ginseng: *in vitro* and *in vivo* studies. *Int J Pharm* 2007;**328**:168−76.
18. Yu J, Xin YF, Gu LQ, Gao HY, Xia LJ, You ZQ, et al. One-month toxicokinetic study of SHENMAI injection in rats. *J Ethnopharmacol* 2014;**154**:391−9.
19. Xia C, Wang G, Sun J, Hao H, Xiong Y, Gu S, et al. Simultaneous determination of ginsenoside Rg1, Re, Rd, Rb1 and ophiopogonin D in rat plasma by liquid chromatography/electrospray ionization mass spectrometric method and its application to pharmacokinetic study of 'SHENMAI' injection. *J Chromatogr B Analyt Technol Biomed Life Sci* 2008;**862**:72−8.
20. Yu J, Gu LQ, Xin YF, Gao HY, Xu XZ, Zhang S, et al. Simultaneous determination and pharmacokinetics of eight ginsenosides by LC−MS/MS after intravenously infusion of 'SHENMAI' injection in dogs. *Pak J Pharm Sci* 2017;**30**:421−7.
21. Sun J, Wang G, Haitang X, Hao L, Guoyu P, Tucker I. Simultaneous rapid quantification of ginsenoside Rg1 and its secondary glycoside Rh1 and aglycone protopanaxatriol in rat plasma by liquid chromatography−mass spectrometry after solid-phase extraction. *J Pharm Biomed Anal* 2005;**38**:126−32.
22. Zhou Y, Zhao B, Wu W, Yang X, Long S, Deng H, et al. Shenmai injection for the treatment of cancer-related fatigue in advanced non-small cell lung cancer patients undergoing chemotherapy: study protocol for a randomized controlled trial. *Trials* 2018;**19**:474−82.
23. Wu JB, Tang YL, Liang XH. Targeting VEGF pathway to normalize the vasculature: an emerging insight in cancer therapy. *OncoTargets Ther* 2018;**11**:6901−9.
24. Huang D, Lan H, Liu F, Wang S, Chen X, Jin K, et al. Anti-angiogenesis or pro-angiogenesis for cancer treatment: focus on drug distribution. *Int J Clin Exp Med* 2015;**8**:8369−76.
25. Liu W, Zhang J, Yao X, Jiang C, Ni P, Cheng L, et al. Bevacizumab-enhanced antitumor effect of 5-fluorouracil *via* upregulation of thymidine phosphorylase through vascular endothelial growth factor A/vascular endothelial growth factor receptor 2-specificity protein 1 pathway. *Cancer Sci* 2018;**109**:3294−304.
26. Weiss A, Bonvin D, Berndsen RH, Scherrer E, Wong TJ, Dyson PJ, et al. Angiostatic treatment prior to chemo- or photodynamic therapy improves anti-tumor efficacy. *Sci Rep* 2015;**5**:8990−7.
27. Goel S, Duda DG, Xu L, Munn LL, Boucher Y, Fukumura D, et al. Normalization of the vasculature for treatment of cancer and other diseases. *Physiol Rev* 2011;**91**:1071−121.
28. Olaleye OE, Niu W, Du FF, Wang FQ, Xu F, Pintusophon S, et al. Multiple circulating saponins from intravenous ShenMai inhibit OATP1Bs *in vitro*: potential joint precipitants of drug interactions. *Acta Pharmacol Sin* 2019;**40**:833−49.
29. Yu J, Gu LQ, Xin YF, Bai YS, Zhang S, Gao HY, et al. Potential accumulation of protopanaxadiol-type ginsenosides in six-months toxicokinetic study of SHENMAI injection in dogs. *Regul Toxicol Pharmacol* 2017;**83**:5−12.
30. Liu R, Hu C, Yang Y, Zhang J, Gao H. Theranostic nanoparticles with tumor-specific enzyme-triggered size reduction and drug release to perform photothermal therapy for breast cancer treatment. *Acta Pharm Sin B* 2019;**9**:410−20.
31. Lin F, Guo X, Lu W. Efficient biotransformation of ginsenoside Rb1 to Rd by isolated Aspergillus versicolor, excreting beta-glucosidase in the spore production phase of solid culture. *Antonie Leeuwenhoek* 2015;**108**:1117−27.
32. Hong H, Cui CH, Kim JK, Jin FX, Kim SC, Im WT. Enzymatic biotransformation of ginsenoside Rb1 and gypenoside XVII into ginsenosides Rd and F2 by recombinant beta-glucosidase from flavobacterium johnsoniae. *J Ginseng Res* 2012;**36**:418−24.
33. Zeng C, He F, Xia C, Zhang H, Xiong Y. Identification of the active components in Shenmai injection that differentially affect Cyp3a4-mediated 1′-hydroxylation and 4-hydroxylation of midazolam. *Drug Metab Dispos* 2013;**41**:785−90.

34. Liu X, Chen L, Liu M, Zhang H, Huang S, Xiong Y, et al. Ginsenoside Rb1 and Rd remarkably inhibited the hepatic uptake of ophiopogonin D in Shenmai injection mediated by OATPs/oatps. *Front Pharmacol* 2018;**9**:957.
35. Hida K, Maishi N, Annan DA, Hida Y. Contribution of tumor endothelial cells in cancer progression. *Int J Mol Sci* 2018;**19**:1272−84.
36. Rohlenova K, Veys K, Miranda-Santos I, de Bock K, Carmeliet P. Endothelial cell metabolism in health and disease. *Trends Cell Biol* 2018;**28**:224−36.
37. Jain RK. Normalizing tumor vasculature with anti-angiogenic therapy: a new paradigm for combination therapy. *Nat Med* 2001;**7**:987−9.
38. Vasudev NS, Reynolds AR. Anti-angiogenic therapy for cancer: current progress, unresolved questions and future directions. *Angiogenesis* 2014;**17**:471−94.
39. Gong X, Qin S. Study progression of anti-angiogenetic therapy and its combination with other agents for the treatment of advanced hepatocellular carcinoma. *Hepatobiliary Surg Nutr* 2018;**7**:466−74.
40. Cheng AL, Cornelio G, Shen L, Price T, Yang TS, Chung IJ, et al. Efficacy, tolerability, and biomarker analyses of once-every-2-weeks cetuximab plus first-line FOLFOX or FOLFIRI in patients with KRAS or all RAS wild-type metastatic colorectal cancer: the phase 2 APEC study. *Clin Colorectal Cancer* 2017;**16**:e73−88.
41. Viallard C, Larrivee B. Tumor angiogenesis and vascular normalization: alternative therapeutic targets. *Angiogenesis* 2017;**20**:409−26.
42. Wu X, Hu W, Lu L, Zhao Y, Zhou Y, Xiao Z, et al. Repurposing vitamin D for treatment of human malignancies *via* targeting tumor microenvironment. *Acta Pharm Sin B* 2019;**9**:203−19.
43. Kim YJ, Yamabe N, Choi P, Lee JW, Ham J, Kang KS. Efficient thermal deglycosylation of ginsenoside Rd and its contribution to the improved anticancer activity of ginseng. *J Agric Food Chem* 2013;**61**:9185−91.
44. Kim BJ. Involvement of melastatin type transient receptor potential 7 channels in ginsenoside Rd-induced apoptosis in gastric and breast cancer cells. *J Ginseng Res* 2013;**37**:201−9.
45. Wang P, Du X, Xiong M, Cui J, Yang Q, Wang W, et al. Ginsenoside Rd attenuates breast cancer metastasis implicating derepressing microRNA-18a-regulated Smad2 expression. *Sci Rep* 2016;**6**:33709−22.
46. Yoon JH, Choi YJ, Cha SW, Lee SG. Anti-metastatic effects of ginsenoside Rd *via* inactivation of MAPK signaling and induction of focal adhesion formation. *Phytomedicine* 2012;**19**:284−92.
47. Zhang E, Shi H, Yang L, Wu X, Wang Z. Ginsenoside Rd regulates the Akt/mTOR/p70S6K signaling cascade and suppresses angiogenesis and breast tumor growth. *Oncol Rep* 2017;**38**:359−67.
48. Missiaen R, Morales-Rodriguez F, Eelen G, Carmeliet P. Targeting endothelial metabolism for anti-angiogenesis therapy: a pharmacological perspective. *Vascul Pharmacol* 2017;**90**:8−18.
49. Park JS, Kim IK, Han S, Park I, Kim C, Bae J, et al. Normalization of tumor vessels by Tie2 activation and Ang2 inhibition enhances drug delivery and produces a favorable tumor microenvironment. *Cancer Cell* 2016;**30**:953−67.
50. Yang H, Lee S, Lee S, Kim K, Yang Y, Kim JH, et al. Sox17 promotes tumor angiogenesis and destabilizes tumor vessels in mice. *J Clin Investig* 2013;**123**:418−31.
51. Lu H, Zhou X, Kwok HH, Dong M, Liu Z, Poon PY, et al. Ginsenoside-Rb1-mediated anti-angiogenesis *via* regulating PEDF and miR-33a through the activation of PPAR-gamma pathway. *Front Pharmacol* 2017;**8**:783.
52. Chan LS, Yue PY, Wong YY, Wong RN. MicroRNA-15b contributes to ginsenoside-Rg1-induced angiogenesis through increased expression of VEGFR-2. *Biochem Pharmacol* 2013;**86**:392−400.
53. Huang YC, Chen CT, Chen SC, Lai PH, Liang HC, Chang Y, et al. A natural compound (ginsenoside Re) isolated from *Panax ginseng* as a novel angiogenic agent for tissue regeneration. *Pharm Res* 2005;**22**:636−46.
54. Dong WW, Zhao J, Zhong FL, Zhu WJ, Jiang J, Wu S, et al. Biotransformation of *Panax ginseng* extract by rat intestinal microflora: identification and quantification of metabolites using liquid chromatography−tandem mass spectrometry. *J Ginseng Res* 2017;**41**:540−7.
55. Tang YC, Zhang Y, Zhou J, Zhi Q, Wu MY, Gong FR, et al. Ginsenoside Rg3 targets cancer stem cells and tumor angiogenesis to inhibit colorectal cancer progression *in vivo*. *Int J Oncol* 2018;**52**:127−38.
56. Kim JW, Jung SY, Kwon YH, Lee JH, Lee YM, Lee BY, et al. Ginsenoside Rg3 attenuates tumor angiogenesis *via* inhibiting bioactivities of endothelial progenitor cells. *Cancer Biol Ther* 2012;**13**:504−15.
57. Shin KO, Seo CH, Cho HH, Oh S, Hong SP, Yoo HS, et al. Ginsenoside compound K inhibits angiogenesis *via* regulation of sphingosine kinase-1 in human umbilical vein endothelial cells. *Arch Pharm Res* 2014;**37**:1183−92.